AMOC Variability in Climate Models and Its Dependence on the Mean State

Brady S Ferster, Alexey V. Fedorov, Juliette Mignot, Éric Guilyardi

Geophysical Research Letters

RESEARCH LETTER
10.1029/2024GL110356

AMOC Variability in Climate Models and Its Dependence on the Mean State

Brady S. Ferster[1,2], Alexey V. Fedorov[1,2], Juliette Mignot[1], and Eric Guilyardi[1,3]

[1]LOCEAN-IPSL, Sorbonne Université, CNRS, IRD, MNHN, Paris, France, [2]Department of Earth and Planetary Sciences, Yale University, New Haven, CT, USA, [3]NCAS-Climate, University of Reading, Reading, UK

Key Points:

- Decadal-to-multidecadal Atlantic Meridional Overturning Circulation (*AMOC*) variability in IPSL-CM6A-LR is driven through subpolar North Atlantic temperature anomalies
- Centennial *AMOC* variability in IPSL-CM6A-LR is driven by salinity in the western subpolar North Atlantic
- The amplitude of decadal-to-multidecadal mode also depends linearly on the mean *AMOC* strength across CMIP6 models

Supporting Information:

Supporting Information may be found in the online version of this article.

Correspondence to:

J. Mignot and B. S. Ferster,
juliette.mignot@locean.ipsl.fr;
brady.ferster@locean.ipsl.fr

Citation:

Ferster, B. S., Fedorov, A. V., Mignot, J., & Guilyardi, E. (2025). *AMOC* variability in climate models and its dependence on the mean state. *Geophysical Research Letters*, *52*, e2024GL110356. https://doi.org/10.1029/2024GL110356

Received 17 MAY 2024
Accepted 26 AUG 2024

Abstract Understanding internal variability of the climate system is critical when isolating internal and anthropogenically forced signals. Here, we investigate the modes of Atlantic Meridional Overturning Circulation (*AMOC*) variability using perturbation experiments with the Institut Pierre-Simon Laplace's (IPSL) coupled model and compare them to Coupled Model Intercomparison Project Phase 6 (CMIP6) pre-industrial control simulations. We identify two characteristic modes of variability—decadal-to-multidecadal (DMD_{var}) and centennial (CEN_{var}). The former is driven largely by temperature anomalies in the subpolar North Atlantic, while the latter is driven by salinity in the western subpolar North Atlantic. The amplitude of each mode scales linearly with the mean *AMOC* strength in the IPSL experiments. The DMD_{var} amplitude correlates well with the *AMOC* mean strength across CMIP6 models, while the CEN_{var} mode does not. These findings suggest that the strength of DMD_{var} depends robustly on the North Atlantic mean state, while the CEN_{var} mode may be model-dependent.

Plain Language Summary Understanding climate natural variability is crucial for distinguishing between changes caused by human activity and climate fluctuations that occur on their own. In this study, we investigate different timescales and patterns of variation in the Atlantic Ocean's circulation system, called the Atlantic meridional overturning circulation (*AMOC*). Using coupled model simulations, we study how the *AMOC* behaves under various conditions. We find two main types of *AMOC* variations: one that occurs over decades to multiple decades, and another that happens over centuries. The shorter-term variation was mainly influenced by changes in temperature and salinity in the western subpolar North Atlantic Ocean, while the longer-term variation is more affected by salinity in the same region. When comparing to other coupled models from the Coupled Model Intercomparison Project Phase 6, the strength of the shorter-term variation is related directly to the overall strength of the overturning circulation, while the longer-term variation does not exhibit the same relationship. This suggests that the shorter-term variation is more consistently tied to the conditions of the North Atlantic Ocean, while the longer-term one might vary depending on the specific coupled climate models.

1. Introduction

The Atlantic Meridional Overturning Circulation (*AMOC*) is a vital component of the Earth's climate system that plays a crucial role in transporting heat, freshwater, and carbon across the Atlantic basin. This large-scale ocean overturning system transports warm surface water from the tropics toward the subpolar North Atlantic, where it exchanges heat with the atmosphere and allows the formation of deep, dense waters that feed a return flow toward the tropics. As a result, the *AMOC* plays a critical role in regulating climate by redistributing heat and freshwater, and influencing the carbon cycle, while variations in its strength and structure can have significant impacts on large-scale climate patterns. Reviews of the *AMOC* dynamics and related large-scale climate impacts can be found in (Buckley & Marshall, 2016 or Weijer et al., 2019).

At decadal and longer timescales, variations in surface buoyancy fluxes play an important role in driving the variability of the *AMOC* by generating density anomalies in the upper ocean in climate models (Kostov et al., 2019; Li et al., 2021; Liu et al., 2019; Polo et al., 2014; Sévellec et al., 2017). These buoyancy fluxes impact the *AMOC* by modifying the density of the upper ocean in the high-latitude North Atlantic region through changes in temperature and salinity. Changes in wind stress can also contribute to the overall variability of the *AMOC* in the subpolar North Atlantic (Kostov et al., 2019; Yeager & Robson, 2017) and subtropical North Atlantic (Zhao & Johns, 2014). Within the subpolar North Atlantic, approximately poleward of ~45°N, variability is largely driven through both buoyancy (i.e., surface fluxes) and mechanical (i.e., wind) forcings

(Larson et al., 2020; Yeager & Danabasoglu, 2014). The buoyancy forcing drives meridionally coherent decadal variability, and the mechanical forcing introduces an asymmetric pattern of variability across the North Atlantic basin (Yeager & Danabasoglu, 2014).

Modeling studies (e.g., Ferster et al., 2022; Menary et al., 2020b; Ortega et al., 2017) have demonstrated that internal buoyancy driven variability originating in the western subpolar North Atlantic may drive *AMOC* variability on decadal timescales and is a major contribution to the decadal and lower-frequencies *AMOC* variability (Muir & Fedorov, 2015, 2017; Oldenburg et al., 2021; Sévellec & Fedorov, 2013, 2015). Moreover, the southward propagation of the buoyancy-driven *AMOC* variability from the subpolar North Atlantic can be damped in the subtropical Atlantic due to mechanical forcing of wind-driven mixing and transports (Baehr et al., 2008; Larson et al., 2020; Rühs et al., 2015; Sévellec et al., 2017).

Sea surface temperature (*SST*) and salinity (*SSS*) variations in the North Atlantic are related to *AMOC* through changes in the buoyancy of the upper ocean in the high-latitude North Atlantic region (Chiang et al., 2021). Low-frequency variations in *AMOC,* signals of decadal-to-multidecadal variability, have been shown to be linked to changes in North Atlantic SST in models (Bjerknes, 1964; Deser et al., 2010; Kushnir, 1994). Large-scale patterns of atmospheric variability, such as the North Atlantic Oscillation (NAO), can drive *AMOC* and *SST* variability through buoyancy fluxes and wind stress forcings (Delworth et al., 2016; Delworth & Zeng, 2016; Mecking et al., 2015). Additionally, variability of the Arctic sea ice (Ferster et al., 2022; Liu et al., 2019; Lobelle et al., 2020; Sévellec et al., 2017) and atmospheric patterns resulting from the tropics (Ferster et al., 2021, 2023a; Hu & Fedorov, 2020; Orihuela-Pinto et al., 2023), and at even lower frequencies, surface freshwater fluxes and salinity have been shown as mechanisms driving *AMOC* decadal to centennial variability (Menary et al., 2012) in models.

As described above, studies have thus shown that the *AMOC* exhibits natural variability on a range of timescales, from years to centuries, and that it can be influenced by both internal and external factors, including changes in ocean and atmospheric circulation patterns, freshwater input, and greenhouse gas concentrations. In the modeling study of Mecking et al. (2015), *AMOC* variability can be separated into three distinct timescales: interannual, multidecadal, and centennial. The role of mechanical forcing proved dominant in interannual variability, the multidecadal variability is driven through density (buoyancy) anomalies in the subpolar North Atlantic, while the centennial mode is attributed to series of quasi-equilibrium states. Although less understood or explored in recent literature, the (multi-) centennial mode of *AMOC* variability is thought to derive from buoyancy anomalies in the subpolar North Atlantic that may originate from the Arctic (Jiang et al., 2021; Waldman et al., 2021) or even from the Southern Ocean (Delworth & Zeng, 2012).

Due to the limited length of *AMOC* observations, much of the scientific literature separating internally driven and externally forced experiments is based on coupled climate models. There have been a number of recent studies focusing on how to separate the forced and internal signals in the Atlantic multidecadal variability (Michel et al., 2022; Qin et al., 2020; Robson et al., 2023) and the *AMOC* (Menary, Robson, et al., 2020; Robson et al., 2022). However, little work has been done exploring the magnitude of variability and its dependence on the mean state within a single model framework. In part, this is due to the challenge of creating experiments with a given model using the same external forcings (i.e., constant or transient) but having different mean *AMOC* strengths, outside the realm of freshwater hosing experiments (i.e., imposing surface freshwater fluxes in the North Atlantic). Therefore, here we investigate a potential dependence of *AMOC* variability on the *AMOC* mean state.

Our approach to analyze internal *AMOC* variability includes two steps. First, we use the tropical Indian Ocean to remotely drive changes in the mean state *AMOC* through a combination of atmospheric teleconnections and oceanic pathways, while using the same model and atmospheric forcings (following the approach of Ferster et al., 2021; Hu & Fedorov, 2019). Second, we compare our results to the pre-industrial control simulations of CMIP6 and further explore the dependence of *AMOC* variability on *AMOC* strength.

2. Methods

2.1. IPSL-CM6A-LR and the Sensitivity Experiments

The experiments utilize the coupled model IPSL-CM6-LR (Boucher et al., 2020; Mignot et al., 2021) from the Institut Pierre-Simon Laplace. This model has an atmospheric grid resolution of 144 × 142 points with 79 layers,

and an ocean configuration on a quasi-isotropic global tripolar grid with 1° nominal resolution, increasing to 1/3° near the equator, and 75 vertical levels varying in thickness from 1 m at the surface to 200 m at depth.

The experimental methods follow Ferster et al. (2021, 2023b), using SST nudging to alter the tropical Indian Ocean temperature (*TIO*) and achieve different *AMOC* mean states. Four experiments applied temperature anomalies of −2°C, −1°C, +1°C, and +2°C (*TIO"x"C*). The *TIO* + 1C and *TIO* + 2C experiments ran for 950 years, *TIO* − 2C for 500 years due to *AMOC* collapse, and *TIO* − 1C for 700 years. The IPSL control simulation spans 1,100 years (*r1i2p1f1*). Ferster et al. (2021) found the IPSL-CM6A-LR model's sensitivity to be approximately 9.4 Sv per 1°C *TIO* warming. This method differs from hosing experiments by using SST gradients to drive *AMOC* changes via tropical teleconnections, maintaining physical consistency of air-sea fluxes in the North Atlantic (Ferster et al., 2023a; Hu & Fedorov, 2019). Consequently, *TIO*-warming (-cooling) experiments result in a warmer, saltier (colder, fresher) North Atlantic mean state and a stronger (weaker) *AMOC* compared to the control.

2.2. Coupled Model Intercomparison Project Phase 6

To further explore mechanisms and robustness across coupled climate models, we include the pre-industrial control simulations of CMIP6 (Eyring et al., 2016) in our study, focusing on simulations with at least 300 years of data. Since most CMIP6 control simulations do not extend to the 1000s of years required to robustly explore centennial variability, we concentrate on multi-decadal analysis to support our sensitivity experiments. In total, 37 different coupled models are used in this study. To ensure robust comparisons, we first analyze all models with at least 300 years of data and then compare a subset of models with at least 900 years of simulation. This approach, balancing more members with shorter timescales against fewer members with longer timescales, has been explored in tropical dynamics (e.g., Lee et al., 2021). This is important to note as CMIP6 models have shown intermittent multi-decadal North Atlantic mechanisms (Bellucci et al., 2022) and the IPSL-CM6A-LR model exhibits time-varying frequency and amplitudes in the (multi-) centennial mode (Povea-Pérez et al., 2024). Therefore, the length of the analyzed data or the background mean state could play a significant role in the analysis. Compared to other CMIP6 models, the IPSL-CM6A-LR is relatively cold and fresh in the subpolar North Atlantic and would result in weaker (multi-) decadal *AMOC* variability (Reintges et al., 2024). A list of the models, the length of simulated years analyzed, and references are provided in Table S1 in Supporting Information S1.

2.3. Defining the Amplitudes of Variability

To begin the analysis of variability, we first define the decadal to multi-decadal (DMD_{var}) and centennial (CEN_{var}) timescales within the IPSL control simulation. Figure 1a shows the low frequency timeseries of the experiments through a 21-year moving mean. Similar to (Ferster et al., 2023b), we will define the quasi-equilibrium in the experiments as starting from the year 200. This is indeed approximately when all experiments reach a new state (shown as dashed vs. solid lines in Figure 1a). The initial 200 years of simulation are thus not considered for the following analyses and only simulated years after 200 are considered to quantify the *AMOC* variability in the new quasi-equilibrium mean state.

To identify the temporal ranges for DMD_{var} and CEN_{var} we use a power spectrum analysis with a variance preserving approach: the power spectral density is multiplied by the frequency and the frequency is shown as logarithmic. Additionally, the analysis applies a multi-taper method (Park et al., 1987; Thomson, 1982; Yu & Fedorov, 2022). The power spectrum analysis (Figure 1b) demonstrates two major bands of *AMOC* variability separated by an interval with low spectral density around 65 years. Accordingly, we define the spectral range of variability for DMD_{var} as 15–65 years and CEN_{var} as 65 years and longer. The definition of these timescales is based on the control simulations and agree with a previous study of Mecking et al. (2015). The two modes of variability are then isolated through a 15–65 years Butterworth band-pass filter and 65 years Butterworth low-pass filter, respectively. The DMD_{var} and CEN_{var} amplitudes are then defined as the respective standard deviation of the filtered timeseries. For both the IPSL and CMIP6 simulations, *AMOC* is defined as the maximum overturning between 40° and 45°N at depths greater than 500 m, representing the subpolar cell of *AMOC*.

In comparing density, components are broken into a temperature (*thermal*) and salinity (*haline*) -driven component. In estimating the contribution to density with this approach, the *thermal* component is estimated by using the time mean salinity with the time-varying temperature, and the *haline* component using the time mean

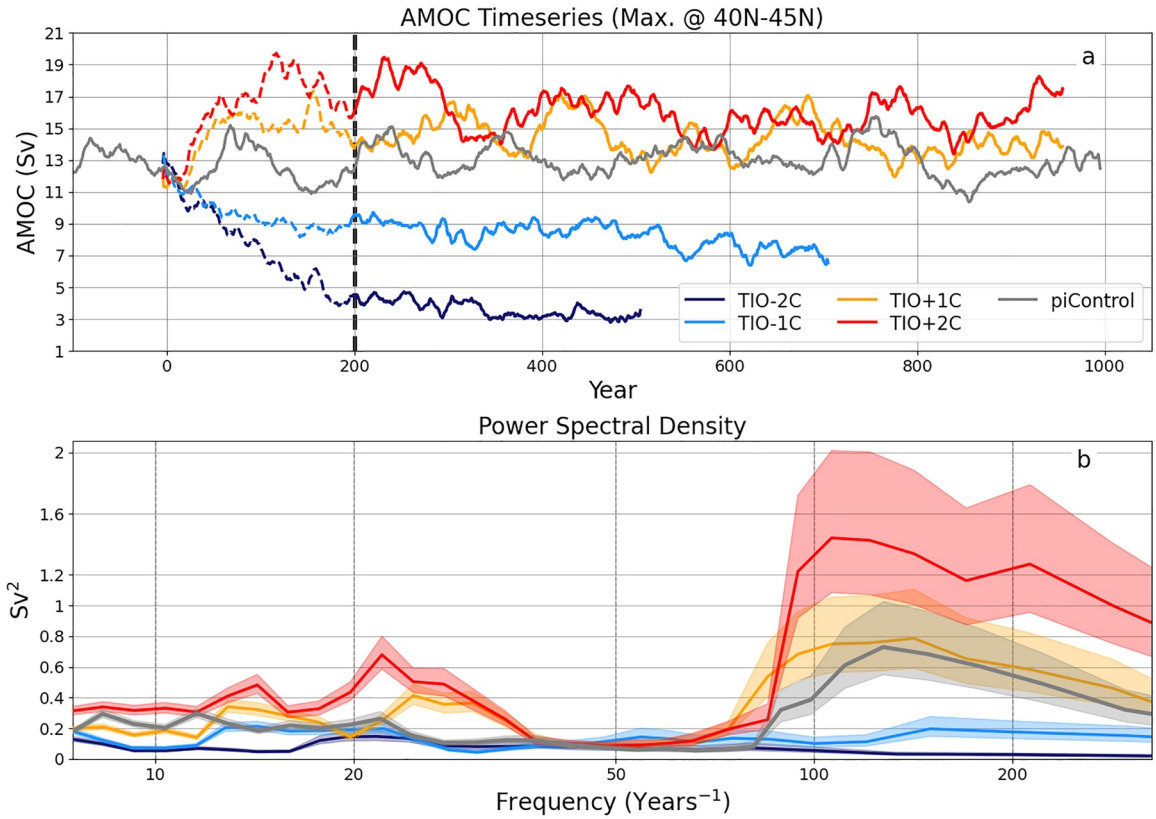

Figure 1. (a) Timeseries of the Atlantic meridional overturning circulation (*AMOC*; Sv) for the IPSL-CM6A-LR perturbation experiments. The *AMOC* strength is defined as the maximum overturning transport between 40° and 45°N at depths greater than 500 m and is plotted with a 21-year moving mean to show the low frequency variability. The initial 200 years are dashed to mark the transient response in the experiments before an approximate quasi-equilibrium is reached. (b) Power spectra of these timeseries for the time interval after year 200. A variance preserving approach is used in which the power spectral density is multiplied by the frequency and the frequency is shown as logarithmic. Note the two broad-maxima in the spectra corresponding to DMD_{var} and CEN_{var}. Shading represents the 99% confidence interval.

temperature and time-varying salinity. This method is similar to Swingedouw et al. (2013). To define significance, we use an alpha of 0.01 to robustly compare to the 99% confidence interval in both parametric and non-parametric significance tests.

3. Results

3.1. *AMOC* Mean State and Amplitudes of Variability

In the IPSL control simulation, the mean *AMOC* is approximately 12.4 ± 1.3 Sv (Figure 1a; mean ± standard deviation), while in the *TIO* + 2C (*TIO* − 2C) experiment, *AMOC* increases (decreases) to approximately 16.0 ± 1.6 Sv (3.6 ± 0.8 Sv). The *TIO* experiments therefore represent four additional *AMOC* mean states compared to the IPSL control, two with decreased and two with increased mean *AMOC* strength. The advantage of this protocol lies in the fact that as opposed to freshwater hosing setups, where buoyancy fluxes in the North Atlantic are directly perturbed, *AMOC* intensity is here modulated from remote perturbation and physical teleconnections. Compared to the control, the experiments with increased mean *AMOC* strength also exhibit larger peaks in the frequencies of DMD_{var} and CEN_{var}, while decreasing amplitude of the signal in a weaker *AMOC* mean strength climate (Figure 1b).

In the control, the amplitudes of DMD_{var} and CEN_{var} are 0.5 and 1.0 Sv, respectively (Figure 2a). In the *TIO* + 2C experiment, their amplitudes increase to 0.6 and 1.2 Sv, respectively, while in the *TIO* − 2C experiment they decrease to 0.3 and 0.5 Sv.

The experiments display a significant relationship between both modes of variability and the mean state *AMOC*. Under a linear assumption, the DMD_{var} thus increases by about 0.022 and CEN_{var} increases by 0.064 Sv per 1 Sv

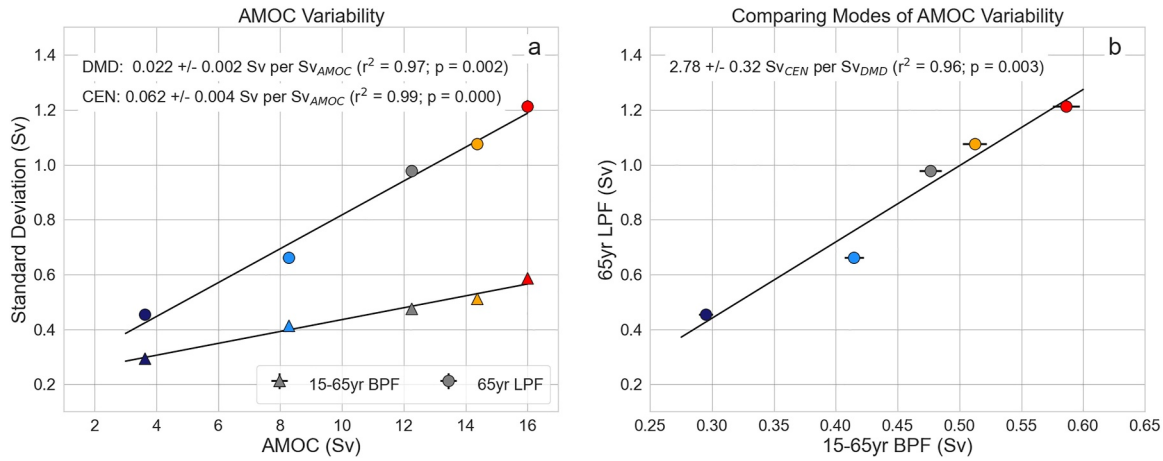

Figure 2. (a) The amplitude of the *AMOC* decadal-to-multidecadal (DMD_{var}) and centennial (CEN_{var}) variability versus the *AMOC* mean strength in the perturbation experiments. DMD_{var} is estimated through a 15–65 years bandpass filter and CEN_{var} through a 65-year lowpass filter applied to the *AMOC* timeseries. (b) Comparing DMD_{var} and CEN_{var} amplitudes: the colored dots indicate different perturbation experiments as shown in Figure 1a. Error bars in panels (a) and (b) represent the 95% confidence interval and the solid lines represents linear regressions, significant at the 95% confidence level. The slope of the regression lines, variance explained (r^2), and p-values are provided in each panel.

of *AMOC* mean. Both regressions are significant at the 99% confidence level, demonstrating the robustness of the linear assumption. When compared to one another, the amplitudes of the two modes scale linearly at roughly 2.8 Sv Sv_{CEN} per Sv_{DMD} (p-value < 0.01; Figure 2b).

3.2. Mechanisms Driving Multi-Decadal and Centennial Variability in the Pre-Industrial Control

The results in Section 3.1 demonstrate that the amplitude of variability in the two lower-frequency modes scale linearly with the mean state *AMOC* strength within the IPSL model. A lag-lead spatial correlation analysis shows a significant positive anomalous winter (JFM; 99% confidence level) ocean mixed layer depth (MLD_{oce}) in the western subpolar and Nordics seas along the coast of Greenland leading the DMD_{var} *AMOC* timeseries by 5 years (Figures 3a and 3b). The annual mean winter MLD_{oce} is contoured on Figure 3a, demonstrating that the positive correlations represent a deepening of the MLD_{oce} over the mean deep convective regions of the IPSL model, in the approximate Labrador and Irminger seas of the western subpolar region of the North Atlantic. On the other hand (Figures 3c and 3d), the low-frequency pattern CEN_{var} *i*s significantly positively correlated with MLD_{oce} throughout the subpolar North Atlantic and Nordic seas, demonstrating a general large spatial-scale deepening MLD_{oce} with the CEN_{var} mode.

There is also an agreement in the patterns of regressing the filtered-*AMOC* on to the winter MLD_{oce} as there are in regressing the filtered-*AMOC* onto density, the temperature and salinity contribution to density (denoted as *thermal* and *haline*) at 200 m depth (Figure S1 in Supporting Information S1). These plots demonstrate the strong spatial similarities between density and *thermal* contributions to *AMOC* variability on decadal-to-multi-decadal timescales throughout the western subpolar region. On centennial timescales, spatial similarities are rather between density and the *haline* component. This suggests different regional and density-driven mechanisms driving the two modes of *AMOC* variability.

To further explore the mechanism and timing for the deepening mixed-layer, lag-lead correlation (Figures 3e–3j) and regression (Figure S2 in Supporting Information S1) analyses are computed using the 200 m depth ocean temperature and salinity and the sea ice area of the defined subpolar North Atlantic and Nordic seas regions using the 1,100 years of the control simulation. Statistics of the correlations and regressions for each basin are further described in Table S2 in Supporting Information S1. The subpolar North Atlantic region is separated by the Reykjanes Ridge and broken into the western subpolar region (Labrador and Irminger seas) and the eastern subpolar (Iceland basin). This separation is motivated by the DMD_{var} demonstrating large regions of positive correlations in the western subpolar (MLD_{oce} deepening) compared with the eastern subpolar in Figure 3a.

The correlation of western subpolar density onto *DMD* signal of *AMOC* peaks at density leading *AMOC* by 3 years ($r = 0.76$, $p < 0.001$; Figure 3e). The *thermal* component in the western subpolar region exhibits a

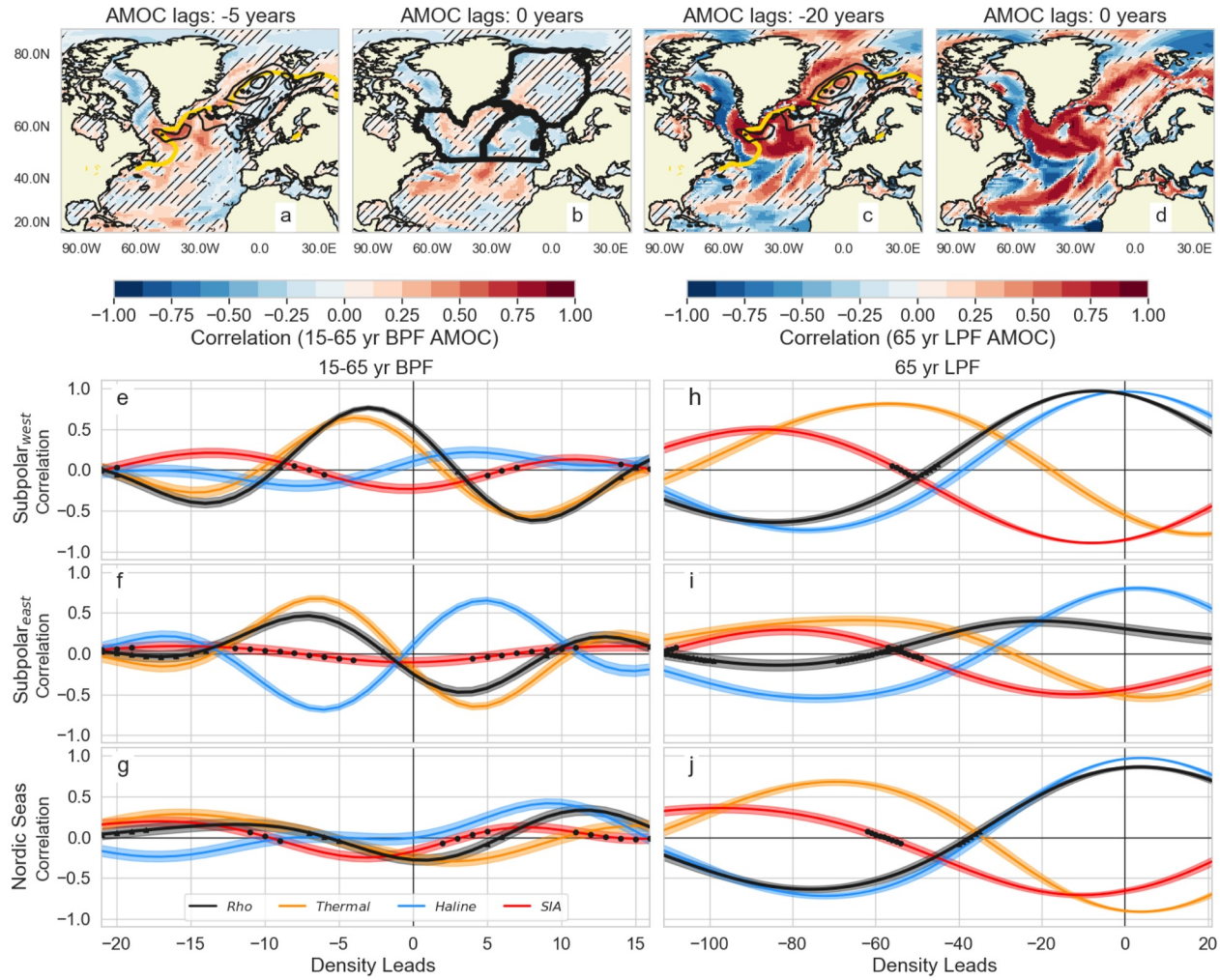

Figure 3. Lag-lead correlations (r) between ocean mixed layer depth and the (a–b) DMD_{var} and (c–d) CEN_{var} filtered *AMOC* timeseries for the IPSL-CM6A-LR pre-industrial control. Hatching represents correlations that are not significant at the 99% confidence level. In panels (a, c) contours represent the time-mean winter (*JFM*) 0.15 concentration Arctic sea ice area (*SIA*) extent (gold) and mean mixed layer depth at 200 m intervals (black). In panel (b) thick black contours mark the western and eastern subpolar North Atlantic regions and the Nordic seas region. (e–g) Lag-lead correlations of density (*Rho*; black) at 200 m depth onto the DMD_{var} timeseries for each region and the contributions from temperature (*Thermal*; orange line) and salinity (*Haline*; blue line) and the basin-averaged *SIA* (red line). Black dots indicate values not significant at the 99% confidence level for *Rho* and shading represents the uncertainty, both accounting for the sample size and autocorrelation. (h–j) Similar regressions but onto the CEN_{var} timeseries. These plots, together with regressions in Figure S2 in Supporting Information S1 demonstrate that density variations in the western subpolar North Atlantic drive DMD_{var} via temperature variations and CEN_{var} via salinity variations. Density variations in the eastern subpolar North Atlantic also contributes to *AMOC* variability, with a large degree of compensation between temperature and salinity in this region. Regressions corresponding to these correlation coefficients are found in Figures S1 and S2 in Supporting Information S1; also see Table S2 in Supporting Information S1.

significant correlation of 0.62 ($p < 0.001$), while the *haline* component is negatively correlated with the density signal (not significant). The density signal leads that of the subpolar sea ice area, which western subpolar sea ice extent is in phase with the *AMOC* (lag-lead = 0 years). *DMD AMOC* variations are thus driven by thermal anomalies in the western subpolar region. In the eastern subpolar, the peak density correlation with *DMD* signal of *AMOC* is at 7 years ($r = 0.47$, $p < 0.001$; Figure 3f). The correlations of the *thermal* and *haline* components of the density signal with *DMD AMOC* are significant but again with opposing signs. Thus, salinity and temperature signals are partly compensating each other, with the temperature effect dominating density variations (see Figure S2b in Supporting Information S1). Although the eastern subpolar North Atlantic density signal leads the *DMD* signal before the western subpolar, the density regression in this region is approximately half the amplitude and thus explains a lower portion of variance (correlation squared, see Table S2 in Supporting Information S1). Within the Nordic Seas (Figure 3g), correlations of density onto the *DMD* signal of *AMOC* peaks after 12 years

($r = 0.33$, $p < 0.001$), while the sea ice area leads by 3 years, indicating that the density anomalies in this region are rather driven by the DMD_{var} of the *AMOC*.

In Figure S3 in Supporting Information S1, the Arctic winter sea ice area is correlated with DMD_{var} at several lags, but the lag-0 spatial correlations are largely confined to the Irminger and Nordic Seas regions. These results demonstrate that the DMD_{var} signal in the subpolar region for the IPSL model is largely driven through temperature anomalies in the western subpolar region and potentially independent of sea ice extent. The lag-lead correlations of basin-averaged timeseries agree with the spatial patterns of *AMOC* regressed onto density in Figure S1 in Supporting Information S1 and demonstrate the importance of the western subpolar temperature contributions in driving DMD_{var} signal of *AMOC*.

The 200 m density signal in the western subpolar region significantly leads the *AMOC* CEN_{var} by 7 years ($r = 0.97$; Figure 3h). The *haline* component correlation similarly peaks near that of density with a peak correlation of 0.93 (Figure S2d in Supporting Information S1), while the *thermal* component is out of phase with the density signal. The density signal of the eastern subpolar North Atlantic leads the CEN_{var} of *AMOC* by approximately 21 years ($r = 0.40$, Figure 3i), however, the *thermal* and *haline* components are compensating in this region. In the eastern subpolar, the peak *thermal* and *haline* signals occur in response to the CEN_{var}, with the *AMOC* leading these two components by 4 years (Figure 2e). The Nordic Seas density signal again lags the CEN_{var} signal of *AMOC* by 4 years ($r = 0.86$; Figure 3j) and both the *thermal* and *haline* components are in phase with the density signal and compensating effects (Figure S2f in Supporting Information S1).

In all three basins, temperature is negatively correlated with the CEN_{var} signal and thus opposes the contributions driven through salinity and density. The strong regression and correlation of salinity in the western subpolar region demonstrate that the centennial signal is likely to be primarily driven through salinity anomalies in this region. Figure S1 in Supporting Information S1 demonstrates spatially the strong density and salinity regressions with CEN_{var} throughout the subpolar North Atlantic, while the temperature contribution exhibits comparatively weaker, negative regressions. Moreover, the sea ice area leads the CEN_{var} signal in all subpolar basins by a decade (Figure S3 in Supporting Information S1), where the Arctic winter sea ice extent is negatively correlated with the CEN_{var} signal and results in reduced sea ice concentrations across the subpolar deep convection regions. Thus, the spatial regressions and correlations support the results that the CEN_{var} signal is driven by salinity and can be related to the Arctic sea ice in the IPSL model (Jiang et al., 2021).

The correlation coefficients and peak lags of DMD_{var} and CEN_{var} are similar across $TIO - 1C$ and $TIO + 1C$ experiments (Figure S4 in Supporting Information S1), the western subpolar region exhibits opposing temperature and salinity signals with the DMD_{var} and CEN_{var} in a cooling climate (see Figures S4a and S4d in Supporting Information S1). These experiments confirm that the DMD_{var} is largely driven through temperature anomalies in the subpolar region and CEN_{var} is salinity driven in the western part of the subpolar North Atlantic, namely the Labrador and Irminger seas, for the IPSL-CM6A-LR model. The robustness across the *TIO* experiments gives credit to the robustness of the mechanisms throughout the IPSL model and varying mean *AMOC* strength and North Atlantic climates. Similar to Reintges et al. (2024), these experiments demonstrate that warmer-saltier mean states with reduced subpolar sea ice results in enhanced variability (*TIO*-warming experiments), albeit here shown in decadal-to-multidecadal and centennial variability. It should also be noted that the correlations and regressions are larger in CEN_{var} than DMD_{var}, which in part is related to bandpass filtering, but has also been shown with atmosphere-ocean Bjerknes compensation for both CEN_{var} and DMD_{var} (Povea-Pérez et al., 2024).

3.3. Variability Across the CMIP6 Pre-Industrial Control Simulations

The logical next question when comparing the modes of variability from IPSL, is whether or not the amplitude of DMD_{var} and CEN_{var} modes of variability are dependent on the *AMOC* mean strength. We investigate this question across CMIP6 models to identify if the same pattern exists across a multi-model analysis. Analyzing 37 pre-industrial control simulations, we demonstrate that there is a significant relationship of *AMOC* strength with the amplitude of DMD_{var} across the CMIP6 ensemble (Figure 4a). In the CMIP6 ensemble, the DMD_{var} significantly increases by about 0.040 Sv per 1 Sv of the *AMOC* mean state (p-value <0.01). This slope, with its associated uncertainty at the 99% confidence interval, is larger in CMIP6 than in the IPSL model slope of DMD_{var} to *AMOC* strength (Figure 2a). This could indicate a model dependence of DMD_{var} sensitivity to *AMOC* strength or reflect uncertainty within the model climate state. Furthermore, a non-parametric permutation test

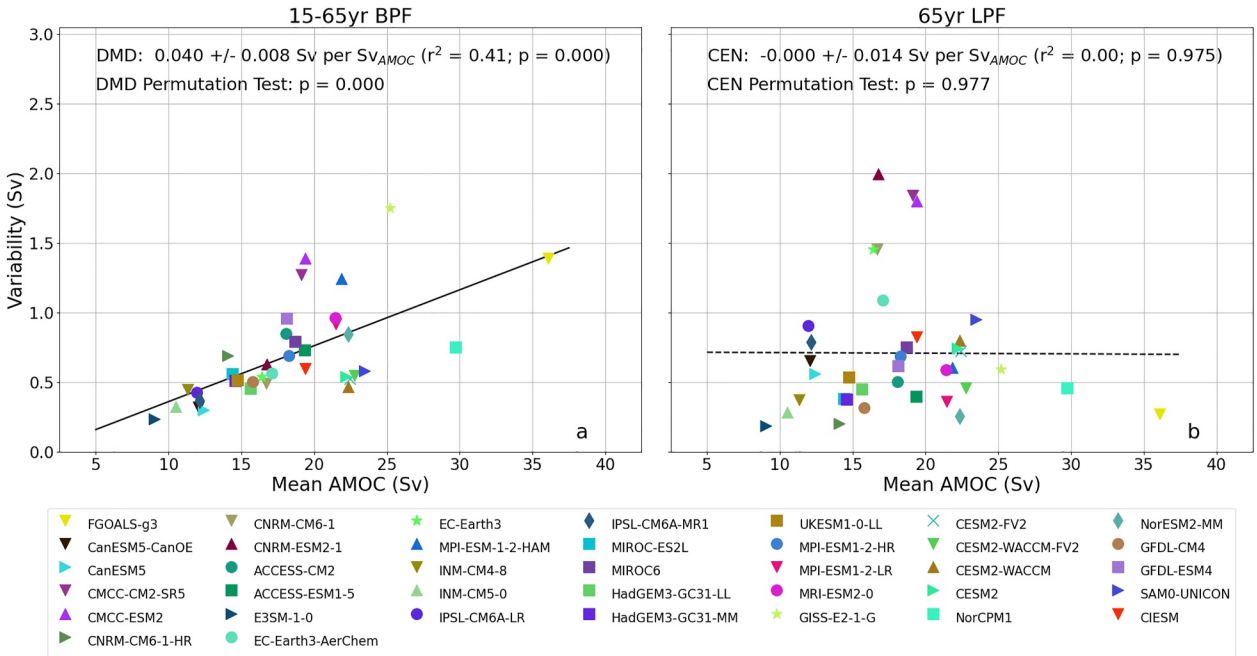

Figure 4. Similar to Figure 2a, but for 37 CMIP6 pre-industrial control simulations. (a) Amplitudes of DMD_{var} and (b) CEN_{var} plotted against the mean *AMOC* strength. At the 99% confidence level, there is a significant relationship between DMD_{var} and the mean *AMOC* with CMIP6 models. Only models with at least 300 years of available data are considered and the timeseries are detrended before the analysis. A similar plot but for models with at least 900 years-long simulations is displayed in Figure S7 in Supporting Information S1. Significance is shown both using a traditional linear regression and a 1,000 resample permutation test.

(Good, 2000) with 1,000 repetitions results in a p-value of less than 0.001, demonstrating the robustness of these results.

In the CEN_{var} of CMIP6 models (Figure 4b), there is no significant trend within the 37-member ensemble. Additionally, a 1000-repetition permutation test further yields a p-value of 0.972, supporting through a non-parametric approach that the slope is not robust and the CEN_{var} is not dependent on *AMOC* mean strength. This result is not surprising, as low frequency centennial signals of *AMOC* are not seen in all models. Strikingly, the coupled models with a relatively large CEN_{var} are those that use the low-resolution ocean model component of NEMO v3.4, like IPSL-CM6A-MR and IPSL-CM6A-LR, CNRM-ESM2 and CNRM-CM6-1 (Waldman et al., 2021), EC-Earth3-AerChem and EC-Earth3 (Meccia et al., 2023; Mehling et al., 2023), and CMCC-CM2-SR5 and CMCC-ESM2. This mode has been described in previous NEMO-based modeling studies, such as Jiang et al. (2021), Waldman et al. (2021), Meccia et al. (2023), and Mehling et al. (2023), that discuss linking the CEN_{var} to a salinity signal originating from the Arctic and propagating into the western subpolar Atlantic. Yet, the exact understanding of the mechanism at play in these models is still an open question in the literature. For example, the GFDL-CM4 and GFDL-ESM4 models do exhibit a centennial mode with its amplitude larger than in other CMIP6 models (see Figures S5–S7 in Supporting Information S1), however it is relatively low when weighted to the mean *AMOC* strength and thought to originate in the Southern Ocean rather than the Arctic (Dunne et al., 2020).

Nevertheless, the focus of this article is not on determining whether the centennial mode is a robust feature or understanding its origins. Instead, we demonstrate that a centennial low-frequency mode does not consistently scale linearly with mean *AMOC* strength across all CMIP6 models or within a subset of models with control simulations longer than 900 years, using a predefined threshold of alpha = 0.01 (Figure 4 and Figure S7 in Supporting Information S1). However, when comparing models grouped by their weighted amplitudes (CEN_{var}) relative to mean *AMOC* strength (Figure S7 in Supporting Information S1), the CEN_{var} indicates linearity with the *AMOC* mean strength in both groups, with low- and high-weighted CEN_{var} at the 95% confidence interval. This suggests that further investigation is needed to explore the possibility that CEN_{var} could scale linearly with mean strength after outliers are removed. What remains robust across the CMIP6 models is the linearity between DMD_{var} and mean *AMOC* strength.

4. Conclusions

In summary, using IPSL-CM6 perturbation experiments we have demonstrated that (a) the decadal to multi-decadal mode of *AMOC* variability (DMD_{var}, 15–65 years) is driven by temperature anomalies in the subpolar North Atlantic. In contrast, the centennial mode (CEN_{var}, 65 + yrs) is largely driven by salinity anomalies in the western subpolar (i.e., Labrador and Irminger seas) (b) The intensity of both low frequency modes of variability (15–65 years band and 65 years and longer) scales linearly with the North Atlantic climatology and mean *AMOC* strength within a single model framework of IPSL-CM6A-LR (c) DMD_{var} amplitude also scales linearly with the mean *AMOC* strength across the CMIP6 pre-industrial control simulations.

The fact that mechanism and timescales of decadal to multi-decadal variability in the IPSL-CM6A-LR are largely controlled through the western subpolar North Atlantic is in agreement with the dense water formation rates (Figure S8 in Supporting Information S1) from Ferster et al. (2021), demonstrating the role of surface heat fluxes in forming increased waters between 27.8 and 28.0 kg m^{-3}. This mechanism could result from the IPSL-CM6A-LR cold-fresh bias, but the impact of the western subpolar density signal on these timescales agrees with previous literature (Muir & Fedorov, 2015, 2017; Sévellec & Fedorov, 2013, 2015; Yeager & Danabasoglu, 2014), even though there can be large differences in the amplitudes and timescales across CMIP models (Menary et al., 2020b; Ortega et al., 2017).

The IPSL-CM6A-LR mechanism of *AMOC* centennial variability driven by salinity anomalies from the western subpolar is supported through the anomalous dense water formations rates in densities larger than 28.1 kg m^{-3} through the surface freshwater flux contribution (Figure S9 in Supporting Information S1) and shown in the results of Jiang et al. (2021) using the same model and Mehling et al. (2023) in models with the NEMO-ocean component. Our results offer new insight into the mechanisms of low frequency *AMOC* variability and dependence on the mean state within coupled climate models. Understanding the details of the connection between the mean state and variability of *AMOC* across CMIP6 models is essential, particularly when trying to quantify the role of *AMOC* on the transient response to anthropogenic forcings in CMIP6 simulations. Further work is required to explore the North Atlantic mean state and origin of the buoyancy forcing across CMIP6 models, specifically whether it is generated through atmospheric teleconnections, air-sea ice interactions within the Arctic, or oceanic transports.

In Kim et al. (2023), differences in sea ice extent within the subpolar North Atlantic in CMIP6 models were shown to result in differences of surface buoyancy fluxes, resulting in different *AMOC* mean states and low-frequency variability. Within the IPSL experiments of Ferster et al. (2021), the *TIO* warming (cooling) simulations resulted in decreased (increased) subpolar North Atlantic sea ice and increased (decreased) dense water formation rates through buoyancy driven surface fluxes, also demonstrating the importance of North Atlantic and Arctic sea ice on the *AMOC* mean state and variability in a single model. Additionally, the results of Yeager et al. (2021), who highlighted the importance of the Labrador Sea region in modeled *AMOC* variability, suggest that much longer direct *AMOC* observations are needed before concluding the role of the Labrador Sea in multidecadal *AMOC* variability in nature versus climate models.

We have demonstrated that decadal-to-multidecadal variability scales linearly with the *AMOC* mean strength in single model experiments and across the CMIP6 pre-industrial control ensemble. Hourdin et al. (2023) showed that different configurations of the IPSL-CM6A-LR model can achieve similar mean states while exhibiting different internal modes. This partially explains the r-squared value of 0.4 (and higher in Figure S7 in Supporting Information S1) across CMIP6 DMD_{var}. There is also inherent uncertainty related to the models' mean state bias and mechanisms driving ocean overturning (i.e., Bellucci et al., 2022; Bellomo & Mehling, 2024; Reintges et al., 2024; Zhao et al., 2024), demonstrated through these perturbation experiments. Future studies should further analyze the thermal and haline components driving variability on multidecadal-to-centennial scales for CMIP6. While the centennial mode's amplitude scales linearly with *AMOC* strength in our experiments, it does not consistently do so across CMIP6 pre-industrial experiments. This implies the need for longer control simulations to better understand internal variability in CMIP models (i.e., Povea-Pérez et al., 2024). We hypothesize that this is because different mechanisms can drive the (multi-) centennial mode in different models and not fully in the present models.

Data Availability Statement

The data sets generated during the experiment are located on the TGCC machine Irene. Several data sets to reproduce the results of the manuscript are published as Ferster, Mignot, et al., 2023c, 2023d (cooling experiments and warming experiments respectively) and details to access the public threads of all the model output for each of the experiments on the TGCC machine are found with the corresponding published data sets. The IPSL and all of the CMIP6 pre-industrial control data sets are publicly available and archived on the CMIP6 ESGF servers (i.e., IPSL: https://esgf-node.ipsl.upmc.fr/search/cmip6-ipsl/). Additional CMIP6 output was obtained through the Earth System Grid Federation (ESGF, 2024) team's python PyClient tool.

Acknowledgments
This research is supported by the ARCHANGE project of the "Make our planet great again" program (ANR-18-MPGA-0001, France). AVF is also supported by Grants from NSF (AGS-2053096, U.S.A.) and DOE (DE-SC0024186, U.S.A.). JM is supported by the JPI climate/JPI ocean ROADMAP project (ANR-19-JPOC-003, France). This work used the HPC resources of TGCC under the allocations provided by GENCI (Grand Equipement National de Calcul Intensif) and benefited from the ESPRI (Ensemble de Services Pour la Recherche l'IPSL) computing and data center (https://mesocentre.ipsl.fr) which is supported by CNRS, Sorbonne University, Ecole Polytechnique and CNES and through national and international grants.

References

Baehr, J., Keller, K., & Marotzke, J. (2008). Detecting potential changes in the meridional overturning circulation at 26°N in the Atlantic. *Climatic Change*, *91*(1–2), 11–27. https://doi.org/10.1007/s10584-006-9153-z

Bellomo, K., & Mehling, O. (2024). Impacts and state-dependence of *AMOC* weakening in a warming climate. *Geophysical Research Letters*, *51*(10), e2023GL107624. https://doi.org/10.1029/2023GL107624

Bellucci, A., Mattei, D., Ruggieri, P., & Famooss Paolini, L. (2022). Intermittent behavior in the *AMOC*-AMV relationship. *Geophysical Research Letters*, *49*(17), e2022GL098771. https://doi.org/10.1029/2022GL098771

Bjerknes, J. (1964). Atlantic air-sea interaction. *Advances in Geophysics*, 1–82. https://doi.org/10.1016/S0065-2687(08)60005-9

Boucher, O., Servonnat, J., Albright, A. L., Aumont, O., Balkanski, Y., Bastrikov, V., et al. (2020). Presentation and evaluation of the IPSL-CM6A-LR climate model. *Journal of Advances in Modeling Earth Systems*, *12*(7), e2019MS002010. https://doi.org/10.1029/2019MS002010

Buckley, M. W., & Marshall, J. (2016). Observations, inferences, and mechanisms of the Atlantic meridional overturning circulation: A review. *Reviews of Geophysics*, *54*(1), 5–63. https://doi.org/10.1002/2015RG000493

Chiang, J. C. H., Cheng, W., Kim, W. M., & Kim, S. (2021). Untangling the relationship between *AMOC* variability and North Atlantic upper-Ocean Temperature and salinity. *Geophysical Research Letters*, *48*(14), e2021GL093496. https://doi.org/10.1029/2021GL093496

Delworth, T. L., & Zeng, F. (2012). Multicentennial variability of the Atlantic meridional overturning circulation and its climatic influence in a 4000 year simulation of the GFDL CM2. 1 climate model. *Geophysical Research Letters*, *39*(13), L13702. https://doi.org/10.1029/2012GL052107

Delworth, T. L., & Zeng, F. (2016). The impact of the North Atlantic Oscillation on climate through its influence on the Atlantic meridional overturning circulation. *Journal of Climate*, *29*(3), 941–962. https://doi.org/10.1175/JCLI-D-15-0396.1

Delworth, T. L., Zeng, F., Vecchi, G. A., Yang, X., Zhang, L., & Zhang, R. (2016). The North Atlantic oscillation as a driver of rapid climate change in the Northern Hemisphere. *Nature Geoscience*, *9*(7), 509–512. https://doi.org/10.1038/ngeo2738

Deser, C., Alexander, M. A., Xie, S.-P., & Phillips, A. S. (2010). Sea surface temperature variability: Patterns and mechanisms. *Annual Review of Marine Science*, *2*(1), 115–143. https://doi.org/10.1146/annurev-marine-120408-151453

Dunne, J. P., Horowitz, L. W., Adcroft, A. J., Ginoux, P., Held, I. M., John, J. G., et al. (2020). The GFDL Earth system model version 4.1 (GFDL-ESM 4.1): Overall coupled model description and simulation characteristics. *Journal of Advances in Modeling Earth Systems*, *12*(11). https://doi.org/10.1029/2019MS002015

Earth System Grid Federation (ESGF) team. (2024). ESGF PyClient. [Software]. https://github.com/ESGF/esgf-pyclient

Eyring, V., Bony, S., Meehl, G. A., Senior, C. A., Stevens, B., Stouffer, R. J., & Taylor, K. E. (2016). Overview of the coupled model Intercomparison project phase 6 (CMIP6) experimental design and organization. *Geoscientific Model Development*, *9*(5), 1937–1958. https://doi.org/10.5194/gmd-9-1937-2016

Ferster, B., Mignot, J., Fedorov, A., & Guilyardi, E. (2023c). Nudging the tropical Indian ocean applied to the IPSL-CM6A-LR model - cooling experiments (version v1) [Dataset]. *Zenodo*. https://doi.org/10.5281/zenodo.7590087

Ferster, B., Mignot, J., Fedorov, A., & Guilyardi, E. (2023d). Nudging the tropical Indian ocean applied to the IPSL-CM6A-LR model - warming experiments (version v1) [Dataset]. *Zenodo*. https://doi.org/10.5281/zenodo.7579970

Ferster, B. S., Borchert, L. F., Mignot, J., Menary, M. B., Cassou, C., & Fedorov, A. V. (2023a). Pantropical Indo-Atlantic temperature gradient modulates multi-decadal *AMOC* variability in models and observations. *Npj Climate and Atmospheric Science*, *6*(1), 165. https://doi.org/10.1038/s41612-023-00489-x

Ferster, B. S., Fedorov, A. V., Guilyardi, E., & Mignot, J. (2023b). The effect of Indian Ocean Temperature on the Pacific trade winds and ENSO. *Geophysical Research Letters*, *50*(20), e2023GL103230. https://doi.org/10.1029/2023GL103230

Ferster, B. S., Fedorov, A. V., Mignot, J., & Guilyardi, E. (2021). Sensitivity of the Atlantic meridional overturning circulation and climate to tropical Indian Ocean warming. *Climate Dynamics*, *5*(0123456789), 1–19. https://doi.org/10.1007/s00382-021-05813-w

Ferster, B. S., Simon, A., Fedorov, A., Mignot, J., & Guilyardi, E. (2022). Slowdown and recovery of the Atlantic meridional overturning circulation and a persistent North Atlantic warming hole induced by Arctic sea ice decline. *Geophysical Research Letters*, *49*(16), e2022GL097967. https://doi.org/10.1029/2022GL097967

Good, P. (2000). Permutation tests: A practical guide to resampling methods for testing hypotheses. In *Springer series in statistics*. Springer-Verlag. Retrieved from https://link.springer.com/book/10.1007/978-1-4757-3235-1

Hourdin, F., Ferster, B., Deshayes, J., Mignot, J., Musat, I., & Williamson, D. (2023). Toward machine-assisted tuning avoiding the underestimation of uncertainty in climate change projections. *Science Advances*, *9*(29), eadf2758. https://doi.org/10.1126/sciadv.adf2758

Hu, S., & Fedorov, A. V. (2019). Indian Ocean warming can strengthen the Atlantic meridional overturning circulation. *Nature Climate Change*, *9*(10), 747–751. https://doi.org/10.1038/s41558-019-0566-x

Hu, S., & Fedorov, A. V. (2020). Indian Ocean warming as a driver of the North Atlantic warming hole. *Nature Communications*, *11*(1), 4785. https://doi.org/10.1038/s41467-020-18522-5

Jiang, W., Gastineau, G., & Codron, F. (2021). Multicentennial variability driven by salinity exchanges between the Atlantic and the Arctic ocean in a coupled climate model. *Journal of Advances in Modeling Earth Systems*, *13*(3), e2020MS002366. https://doi.org/10.1029/2020MS002366

Kim, H.-J., An, S.-I., Park, J.-H., Sung, M.-K., Kim, D., Choi, Y., & Kim, J.-S. (2023). North Atlantic Oscillation impact on the Atlantic meridional overturning circulation shaped by the mean state. *Npj Climate and Atmospheric Science*, *6*(1), 25. https://doi.org/10.1038/s41612-023-00354-x

Kostov, Y., Johnson, H. L., & Marshall, D. P. (2019). *AMOC* sensitivity to surface buoyancy fluxes: The role of air-sea feedback mechanisms. *Climate Dynamics*, *53*(7–8), 4521–4537. https://doi.org/10.1007/s00382-019-04802-4

Kushnir, Y. (1994). Interdecadal variations in North Atlantic sea surface temperature and associated atmospheric conditions. *Journal of Climate*, *7*(1), 141–157. https://doi.org/10.1175/1520-0442(1994)007<0141:IVINAS>2.0.CO;2

Larson, S. M., Buckley, M. W., & Clement, A. C. (2020). Extracting the buoyancy-driven Atlantic meridional overturning circulation. *Journal of Climate*, *33*(11), 4697–4714. https://doi.org/10.1175/JCLI-D-19-0590.1

Lee, J., Planton, Y. Y., Gleckler, P. J., Sperber, K. R., Guilyardi, E., Wittenberg, A. T., et al. (2021). Robust evaluation of ENSO in climate models: How many ensemble members are needed? *Geophysical Research Letters*, *48*(20), e2021GL095041. https://doi.org/10.1029/2021GL095041

Li, H., Fedorov, A., & Liu, W. (2021). *AMOC* stability and diverging response to Arctic sea ice decline in two climate models. *Journal of Climate*, 1–47. https://doi.org/10.1175/JCLI-D-20-0572.1

Liu, W., Fedorov, A., & Sévellec, F. (2019). The mechanisms of the Atlantic meridional overturning circulation slowdown induced by Arctic sea ice decline. *Journal of Climate*, *32*(4), 977–996. https://doi.org/10.1175/JCLI-D-18-0231.1

Lobelle, D., Beaulieu, C., Livina, V., Sévellec, F., & Frajka-Williams, E. (2020). Detectability of an *AMOC* decline in Current and projected climate changes. *Geophysical Research Letters*, *47*(20), e2020GL089974. https://doi.org/10.1029/2020GL089974

Meccia, V. L., Fuentes-Franco, R., Davini, P., Bellomo, K., Fabiano, F., Yang, S., & von Hardenberg, J. (2023). Internal multi-centennial variability of the Atlantic meridional overturning circulation simulated by EC-Earth3. *Climate Dynamics*, *60*(11–12), 3695–3712. https://doi.org/10.1007/s00382-022-06534-4

Mecking, J. V., Keenlyside, N. S., & Greatbatch, R. J. (2015). Multiple timescales of stochastically forced North Atlantic ocean variability: A model study. *Ocean Dynamics*, *65*(9–10), 1367–1381. https://doi.org/10.1007/s10236-015-0868-0

Mehling, O., Bellomo, K., Angeloni, M., Pasquero, C., & von Hardenberg, J. (2023). High-latitude precipitation as a driver of multicentennial variability of the *AMOC* in a climate model of intermediate complexity. *Climate Dynamics*, *61*(3–4), 1519–1534. https://doi.org/10.1007/s00382-022-06640-3

Menary, M. B., Jackson, L. C., & Lozier, M. S. (2020). Reconciling the relationship between the *AMOC* and Labrador Sea in OSNAP observations and climate models. *Geophysical Research Letters*, *47*(18), e2020GL089793. https://doi.org/10.1029/2020GL089793

Menary, M. B., Park, W., Lohmann, K., Vellinga, M., Palmer, M. D., Latif, M., & Jungclaus, J. H. (2012). A multimodel comparison of centennial Atlantic meridional overturning circulation variability. *Climate Dynamics*, *38*(11–12), 2377–2388. https://doi.org/10.1007/s00382-011-1172-4

Menary, M. B., Robson, J., Allan, R. P., Booth, B. B. B., Cassou, C., Gastineau, G., et al. (2020). Aerosol-forced *AMOC* changes in CMIP6 historical simulations. *Geophysical Research Letters*, *47*(14), e2020GL088166. https://doi.org/10.1029/2020GL088166

Michel, S. L. L., Swingedouw, D., Ortega, P., Gastineau, G., Mignot, J., McCarthy, G., & Khodri, M. (2022). Early warning signal for a tipping point suggested by a millennial Atlantic Multidecadal Variability reconstruction. *Nature Communications*, *13*(1), 5176. https://doi.org/10.1038/s41467-022-32704-3

Mignot, J., Hourdin, F., Deshayes, J., Boucher, O., Gastineau, G., Musat, I., et al. (2021). The tuning strategy of IPSL-CM6A-LR. *Journal of Advances in Modeling Earth Systems*, *13*(5), 1–34. https://doi.org/10.1029/2020ms002340

Muir, L. C., & Fedorov, A. V. (2015). How the *AMOC* affects ocean temperatures on decadal to centennial timescales: The North Atlantic versus an interhemispheric seesaw. *Climate Dynamics*, *45*(1–2), 151–160. https://doi.org/10.1007/s00382-014-2443-7

Muir, L. C., & Fedorov, A. V. (2017). Evidence of the *AMOC* interdecadal mode related to westward propagation of temperature anomalies in CMIP5 models. *Climate Dynamics*, *48*(5–6), 1517–1535. https://doi.org/10.1007/s00382-016-3157-9

Oldenburg, D., Wills, R. C. J., Armour, K. C., Thompson, L., & Jackson, L. C. (2021). Mechanisms of low-frequency variability in North Atlantic ocean heat transport and *AMOC*. *Journal of Climate*, 1–68. https://doi.org/10.1175/JCLI-D-20-0614.1

Orihuela-Pinto, B., Santoso, A., England, M. H., & Taschetto, A. S. (2023). Coupled feedbacks from the tropical Pacific to the Atlantic meridional overturning circulation. *Geophysical Research Letters*, *50*(20), e2023GL103250. https://doi.org/10.1029/2023GL103250

Ortega, P., Robson, J., Sutton, R. T., & Andrews, M. B. (2017). Mechanisms of decadal variability in the Labrador Sea and the wider North Atlantic in a high-resolution climate model. *Climate Dynamics*, *49*(7–8), 2625–2647. https://doi.org/10.1007/s00382-016-3467-y

Park, J., Lindberg, C. R., & Vernon, F. L. (1987). Multitaper spectral analysis of high-frequency seismograms. *Journal of Geophysical Research*, *92*(B12), 12675–12684. https://doi.org/10.1029/JB092iB12p12675

Polo, I., Robson, J., Sutton, R., & Balmaseda, M. A. (2014). The importance of wind and buoyancy forcing for the boundary density variations and the Geostrophic component of the *AMOC* at 26°N. *Journal of Physical Oceanography*, *44*(9), 2387–2408. https://doi.org/10.1175/JPO-D-13-0264.1

Povea-Pérez, Y., Guilyardi, É., Fedorov, A. V., & Ferster, B. (2024). The central role of the Atlantic meridional overturning circulation in the Bjerknes compensation. *Climate Dynamics*, *62*(1), 575–587. https://doi.org/10.1007/s00382-023-06926-0

Qin, M., Dai, A., & Hua, W. (2020). Quantifying contributions of internal variability and external forcing to Atlantic multidecadal variability since 1870. *Geophysical Research Letters*, *47*(22), e2020GL089504. https://doi.org/10.1029/2020GL089504

Reintges, A., Robson, J. I., Sutton, R., & Yeager, S. G. (2024). Subpolar North Atlantic mean state affects the response of the Atlantic meridional overturning circulation to the North Atlantic Oscillation in CMIP6 models. *Journal of Climate*. https://doi.org/10.1175/JCLI-D-23-0470.1

Robson, J., Menary, M. B., Sutton, R. T., Mecking, J., Gregory, J. M., Jones, C., et al. (2022). The role of anthropogenic Aerosol forcing in the 1850–1985 strengthening of the *AMOC* in CMIP6 historical simulations. *Journal of Climate*, *35*(20), 3243–3263. https://doi.org/10.1175/JCLI-D-22-0124.1

Robson, J., Sutton, R., Menary, M. B., & Lai, M. W. K. (2023). Contrasting internally and externally generated Atlantic Multidecadal Variability and the role for *AMOC* in CMIP6 historical simulations. *Philosophical Transactions of the Royal Society A: Mathematical, Physical & Engineering Sciences*, *381*(2262), 20220194. https://doi.org/10.1098/rsta.2022.0194

Rühs, S., Getzlaff, K., Durgadoo, J. V., Biastoch, A., & Böning, C. W. (2015). On the suitability of North Brazil Current transport estimates for monitoring basin-scale *AMOC* changes. *Geophysical Research Letters*, *42*(19), 8072–8080. https://doi.org/10.1002/2015GL065695

Sévellec, F., & Fedorov, A. V. (2013). The leading, interdecadal eigenmode of the Atlantic meridional overturning circulation in a realistic ocean model. *Journal of Climate*, *26*(7), 2160–2183. https://doi.org/10.1175/JCLI-D-11-00023.1

Sévellec, F., & Fedorov, A. V. (2015). Optimal excitation of *AMOC* decadal variability: Links to the subpolar ocean. *Progress in Oceanography*, *132*, 287–304. https://doi.org/10.1016/j.pocean.2014.02.006

Sévellec, F., Fedorov, A. V., & Liu, W. (2017). Arctic sea-Ice decline weakens the Atlantic meridional overturning circulation. *Nature Climate Change*, *7*(8), 604–610. https://doi.org/10.1038/NCLIMATE3353

Swingedouw, D., Mignot, J., Labetoulle, S., Guilyardi, E., & Madec, G. (2013). Initialisation and predictability of the *AMOC* over the last 50 years in a climate model. *Climate Dynamics*, *40*(9), 2381–2399. https://doi.org/10.1007/s00382-012-1516-8

Thomson, D. J. (1982). Spectrum estimation and harmonic analysis. *Proceedings of the IEEE*, *70*(9), 1055–1096. https://doi.org/10.1109/PROC.1982.12433

Waldman, R., Hirschi, J., Voldoire, A., Cassou, C., & Msadek, R. (2021). Clarifying the relation between *AMOC* and thermal wind: Application to the centennial variability in a coupled climate model. *Journal of Physical Oceanography*, *51*(2), 343–364. https://doi.org/10.1175/JPO-D-19-0284.1

Weijer, W., Cheng, W., Drijfhout, S. S., Fedorov, A. V., Hu, A., Jackson, L. C., et al. (2019). Stability of the Atlantic meridional overturning circulation: A review and synthesis. *Journal of Geophysical Research: Oceans*, *124*(8), 5336–5375. https://doi.org/10.1029/2019JC015083

Yeager, S., Castruccio, F., Chang, P., Danabasoglu, G., Maroon, E., Small, J., et al. (2021). An outsized role for the Labrador Sea in the multidecadal variability of the Atlantic overturning circulation. *Science Advances*, *7*(41), eabh3592. https://doi.org/10.1126/sciadv.abh3592

Yeager, S., & Danabasoglu, G. (2014). The origins of late-Twentieth-century variations in the large-scale North Atlantic circulation. *Journal of Climate*, *27*(9), 3222–3247. https://doi.org/10.1175/JCLI-D-13-00125.1

Yeager, S. G., & Robson, J. I. (2017). Recent progress in understanding and predicting Atlantic decadal climate variability. *Current Climate Change Reports*, *3*(2), 112–127. https://doi.org/10.1007/s40641-017-0064-z

Yu, S., & Fedorov, A. V. (2022). The essential role of westerly wind bursts in ENSO dynamics and extreme events quantified in model "wind stress shaving" experiments. *Journal of Climate*, *35*(22), 1–62. https://doi.org/10.1175/jcli-d-21-0401.1

Zhao, A., Robson, J., Sutton, R., Lai, M. W., Mecking, J. V., Yeager, S., & Petit, T. (2024). Large diversity in *AMOC* internal variability across NEMO-based climate models. *Climate Dynamics*, *62*(5), 1–20. https://doi.org/10.1007/s00382-023-07069-y

Zhao, J., & Johns, W. (2014). Wind-forced interannual variability of the Atlantic meridional overturning circulation at 26.5°N. *Journal of Geophysical Research: Oceans*, *119*(4), 2403–2419. https://doi.org/10.1002/2013JC009407